CrossMark

ORIGINAL PAPER

Stability analysis of complex rock slopes reinforced with prestressed anchor cables and anti-shear cavities

Jinfeng Bi[1] · Xianqi Luo[1] · Haitao Zhang[1] · Hui Shen[2]

Abstract To evaluate the stability of reinforced complex rock slopes, an evaluation method for slope stability is proposed in this paper. In the proposed method, the force equilibrium of the potential slide mass is analyzed by treating the traction on the potential failure surface as an external force. The potential sliding direction is assumed to be the opposite direction of the resultant shear force on the potential failure surface, and the factor of safety is defined as the ratio of the available resisting force to the actual mobilized force. Through classic cases, the proposed method successfully predicts the stability of a slope critical to failure, and is compared with the traditional methods. Finally, the proposed method is used for a stability analysis of the left bank slope of the Jinping first stage hydropower station, considering two main reinforcing measures, prestressed anchor cables, and anti-shear cavities. Results indicate that the effects of the anti-shear cavities are more positively significant than the effects of the prestressed anchor cables. The safety factor is remarkably increased by the anti-shear cavities, which validates the importance of anti-shear cavities on slope stability.

Introduction

The stability of rock slopes is principally determined by structural discontinuities in the rock mass (Piteau 1972). Fractures and joints increase the complexity of the rock-slope structures, which makes the stability analysis of rock slopes more difficult than that for soil slopes.

Numerous investigations have been performed to analyze the slope stability. The limit equilibrium method (LEM) is the most commonly utilized method for geotechnical stability analyses. Two-dimension (2D) LEMs have been extensively studied for decades (Bishop 1955; Price and Morgenstern 1968; Janbu 1975; Spencer 1976; Sarma 1979) and applied in various circumstances (Lu et al. 2015; Xia et al. 2015; Sun et al. 2016, 2017). Duncan (1996) summarized the development of the LEMs and noted the conditions in which three-dimension (3D) analysis should be used. Kalatehjari and Ali (2013) reviewed 3D slope stability analyses based on the LEM and summarized the limitations of most 3D LEMs, such as engaging with the general shape of slopes, using unreliable theoretical background, ignoring the direction of sliding and restricting the shape of slip surface. Despite their limitations, LEMs are an effective tool for slope stability analyses due to their simplicity and existing availability in the literature (Kelesoglu 2016). Another common tool for geotechnical stability analyses is the strength reduction method (SRM), which was developed by Zienkiewicz et al. (1975). The SRM has been widely applied for the stability analyses of both soil and rock slopes with the development of computing technology (Dawson et al. 2000; Roosta et al. 2005; Hammah et al. 2007;

✉ Xianqi Luo
luoxianqi@sjtu.edu.cn

1   School of Naval Architecture, Ocean and Civil Engineering, Shanghai Jiaotong University, Shanghai 200240, People's Republic of China

2   Faculty of Civil Engineering and Urban Construction, Jiujiang University, Jiujiang 332005, People's Republic of China

Nian et al. 2012; Li et al. 2015a, b; Gupta et al. 2015). Both the LEM and SRM have recently been used to analyze the effects of reinforcements such as anchors (Zhu et al. 2005; Su et al. 2014), soil retaining walls (Chen et al. 2014) and piles (Ausilio et al. 2001; Won et al. 2005; Wei and Cheng 2009) on the slope stability.

Most case studies based on LEMs and SRMs have utilized 2D or simplified 3D models. For 3D complex rock slopes, the sliding mass would be divided into columns in LEMs due to the irregular sliding surface. If there are reinforcement measures, it cannot be avoided that the rock columns will cut through the reinforcing structures on the potential sliding surface or at the intercolumn boundaries. It would be too complicated to conduct the force balance analysis for each column if the interaction mechanism between the rock masses and the reinforcing structures under different conditions is not clear. Therefore, analyzing the stability and reinforcement effects is difficult with LEMs. If the strength of the whole 3D complex rock slope is reduced by SRMs, it is probably that the rock masses or structural planes reach the critical state before the potential sliding surface fails. In addition, SRMs are time-consuming and sensitive to convergence criteria, boundary conditions and the mesh quality (Wei and Cheng 2009). To overcome these limitations of LEMs and SRMs, Ge (2010) put forward a new method based on the fact that forces act as vectors, which is called the vector sum method (VSM). In the VSM, force analysis is conducted on the potential failure surface, and the influence of the potential sliding direction on the safety factor is considered. However, the shear stress and normal stress will be different according to the choice of the potential failure surface. Moreover, the resultant force of the normal stress acting on the potential failure surface due to the base rock is always regarded as a resistant force in the VSM. However, it should be regarded as a sliding force if its projection is opposite to the potential sliding direction.

Inspired by the VSM, a modified slope stability analysis method is proposed. The potential sliding mass is separated from the base rock to conduct the static force equilibrium analysis. The tractions of the potential failure surface are treated as external forces. In addition, the normal stress on the potential failure surface acts as a resistant force or a sliding force. Due to the projection of the resistance, the safety factor is lower than that calculated by the LEM, which is advantageous for engineering practices.

The proposed method is applied on the left bank slope of the Jinping first stage hydropower station. Because of its structural complexities and construction difficulties, this slope has attracted much attention from researchers. Qi et al. (2004, 2010) analyzed the mechanisms of deep cracks and their influence on the stability

of the slope. Sun et al. (2015) used key block theory and studied the stability of the slope using the LEM. Huang et al. (2010) researched the stability of the slope based on geological analyses under earthquake and heavy-rain conditions. Li et al. (2015a) explored the effects of prestressed anchor cables and anti-shear cavities using a reliability analysis. In this paper, these two reinforcements are also considered during the excavation process. The qualitative assessment of the effects of reinforcement is consistent with the conclusions found by Li et al. (2015a) which validates the applicability of the proposed evaluation method for the slope stability.

Evaluation method of slope stability

Method

For complex rock slopes, Fig. 1 shows a potential sliding mass, Ω, separated from the base rock, with a potential failure surface, Γ_s.

In Fig. 1, σ is the stress tensor on Γ_s, and $\mathbf{n}$ is the outer unit normal vector to Γ_s. Then, the normal stress on Γ_s can be obtained by:

$$\sigma_{\mathbf{n}} = (\sigma \cdot \mathbf{n} \cdot \mathbf{n})\mathbf{n} \tag{1}$$

Therefore, the shear stress is:

$$\tau = \sigma \cdot \mathbf{n} - \sigma_{\mathbf{n}} \tag{2}$$

Integrating $\sigma_{\mathbf{n}}$ and τ along Γ_s, we can obtain the resultant force of $\sigma_{\mathbf{n}}$

$$\mathbf{N} = \int_{\Gamma_s} \sigma_{\mathbf{n}} dS \tag{3}$$

and the resultant force of τ

$$\mathbf{T} = \int_{\Gamma_s} \tau dS \tag{4}$$

According to the centroid motion theorem, the resultant forces can be considered to be acting on the centre of mass, G, of the potential sliding mass. For the equilibrium of forces just before the slope failure, another force $\mathbf{V}$ must exist such that

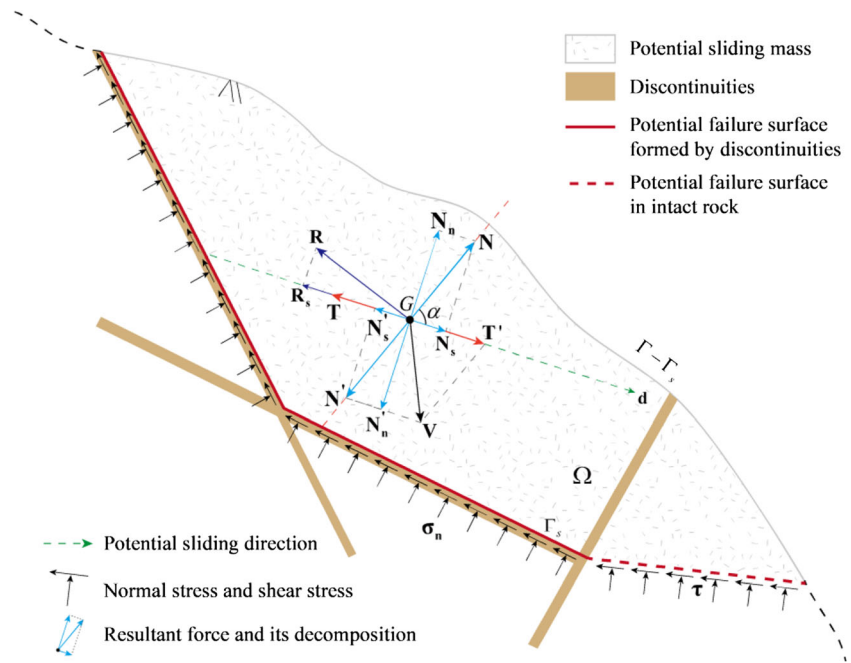$$\mathbf{V} = \int_{\Omega} \mathbf{q_v} dV + \int_{\Gamma - \Gamma_s} \mathbf{q_s} dS \tag{5}$$

which can be decomposed to

$$\mathbf{N}' = -\mathbf{N} \tag{6}$$

and

$$\mathbf{T}' = -\mathbf{T} \tag{7}$$

Fig. 1 Force equilibrium analysis of the potential sliding mass

where Γ represents the entirety of the boundaries of the domain Ω, $\mathbf{q_v}$ is volume of the forces acting on Ω, and $\mathbf{q_s}$ represents the surface forces acting on the ground surface Γ-Γ_s.

According to the Mohr–Coulomb criterion, under a certain stress state, the resisting shear strength on Γ_s is

$$\sigma_r = (c + h|\sigma_n|\tan\phi)\frac{\tau}{|\tau|} \tag{8}$$

in which the resultant force is

$$\mathbf{R} = \int_{\Gamma_s} \sigma_r dS \tag{9}$$

where c and ϕ are the cohesion and friction angles of the material on Γ_s, respectively, and h is a coefficient based on the stress state of Γ_s:

$$h = \begin{cases} 1 & for \quad \sigma_n \cdot n \leq 0 \\ 0 & for \quad \sigma_n \cdot n > 0 \end{cases} \tag{10}$$

It should be noted that c and ϕ are functions of location, which are different on different parts of the potential sliding surface. They should be determined by the filler material for the parts in discontinuities and by the relevant rock masses when the potential sliding surface cuts through the rocks.

Although σ_r has the same direction with τ at every point on Γ_s, the direction of $\mathbf{R}$ may be different from that of $\mathbf{T}$. It is assumed that the movement tendency of the potential sliding mass is translation. There are two options for the transient potential sliding direction, $\mathbf{d}$: the inverse direction of $\mathbf{T}$ and the direction of $\mathbf{R}$. If it becomes the

former, the prediction of the safety factor is conservative compared to the result of the latter. Therefore, the transient potential sliding direction, $\mathbf{d}$, is assumed to be the opposite direction of $\mathbf{T}$, so that

$$\mathbf{d} = -\frac{\mathbf{T}}{|\mathbf{T}|} \tag{11}$$

Considering the condition in Fig. 1, the angle α between $\mathbf{N}$ and $\mathbf{T'}$ is less than 90°, which means that $\mathbf{N}$ has a positive component on the potential sliding direction after orthogonal decomposition. However, an obtuse α is possible. In this situation, $\mathbf{N}$ will serve as a resistant force, and $\mathbf{N'}$ will become a sliding force. Therefore, the total sliding force of the potential sliding mass is

$$\mathbf{F_s} = \begin{cases} \mathbf{T'} + (\mathbf{N} \cdot \mathbf{d})\mathbf{d} & for \quad \mathbf{N} \cdot \mathbf{T'} \geq 0 \\ \mathbf{T'} + (\mathbf{N'} \cdot \mathbf{d})\mathbf{d} & for \quad \mathbf{N} \cdot \mathbf{T'} < 0 \end{cases} \tag{12}$$
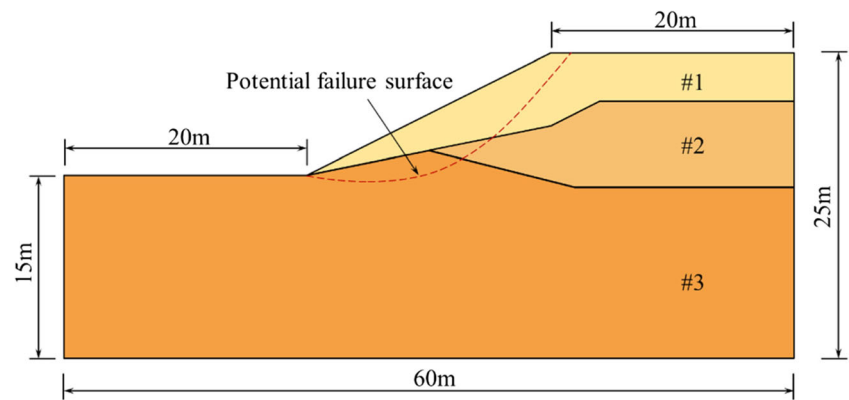
The overall resistance acting on Ω should be

$$\mathbf{F_r} = \begin{cases} (\mathbf{R} \cdot \mathbf{d} + \mathbf{N'} \cdot \mathbf{d})(-\mathbf{d}) & for \quad \mathbf{N} \cdot \mathbf{T'} \geq 0 \\ (\mathbf{R} \cdot \mathbf{d} + \mathbf{N} \cdot \mathbf{d})(-\mathbf{d}) & for \quad \mathbf{N} \cdot \mathbf{T'} < 0 \end{cases} \tag{13}$$

Because of Eqs. (6) and (7), Eqs. (12) and (13) can be simplified as:

$$\mathbf{F_s} = (|\mathbf{T}| + |\mathbf{N} \cdot \mathbf{d}|)\mathbf{d} \tag{14}$$

$$\mathbf{F_r} = (|\mathbf{R} \cdot \mathbf{d}| + |\mathbf{N} \cdot \mathbf{d}|)(-\mathbf{d}) \tag{15}$$

Fig. 2 EX1(a) and EX1(c) of the ACAD

The safety factor can be obtained as:

$$k = \frac{|\mathbf{F_r}|}{|\mathbf{F_s}|} \qquad (16)$$

Remark 1: The force **V** and its components, **N'** and **T'**, are virtually defined for the derivation of k and do not need to be calculated out. The mass centre also does not need to be determined because its location does not affect the result of k.

Remark 2: The derivation of the proposed method is based on tensor analysis. Although a 2D schematic diagram is used to illustrate the relationships among different forces, all the parameters and variables are not distinguished between 2D and 3D situations. The only difference in 2D and 3D slopes is the order of the stress tensor $\boldsymbol{\sigma}$. Therefore, all the previous equations can be applied both in 2D and 3D cases without any change.

A case study for comparison

For a slope critical to failure, the safety factors calculated from different methods should be very close to 1. However, for a safe slope, the safety factors will vary from method to method.

To examine the proposed slope stability analysis method for slopes in critical states and safe states, two examples, EX1(a) and EX1(c), released by the Association for CAD of Australia (ACAD) (Donald and Giam 1992) are analyzed. The schematic plot of EX1(c) is shown in Fig. 2. Problem EX1(a) shares the same dimensions as the EX1(c) slope with a uniform material. The parameters of the soils are listed in Table 1. The safety factors of EX1(a) and EX1(c) were calculated using different methods together with the proposed method, and the results are shown in Table 2.

As seen in Table 2, the stability evaluation of the proposed method is consistent with the conventional LEMs. When the slope approached a critical state, the factor of safety obtained from the proposed method was sufficiently close to 1 as well as the LEM results. This means that the proposed method can well distinguish whether a slope is safe or not. For EX1(c), compared with the Bishop method and the Janbu method, the relative differences were 8.7 and 3.2%, respectively. The reason why the safety factor of the proposed method is smaller than those of LEMs are: (1) in the proposed method, the resistant forces on the potential sliding surface are all projected onto a potential sliding direction along the resultant sliding force, which leads to a reduction of the numerator in the right hand side of Eq. (16); (2) there is a same addition for both the sliding force and the resistant force due to the normal force on the potential sliding surface; if both the numerator and denominator of the safety factor k add a same positive number when $k > 1$, k will become smaller. Therefore, the proposed method

Table 1 Soil parameters of the EX1(a) and EX1(c) slope

Soil	c (kPa)	φ (°)	γ (kN/m³)	E (MPa)	n
EX1(a)	3.0	19.6	20	10.0	0.25
#1 in EX1(c)	0	38.0	19.5	10.0	0.25
#2 in EX1(c)	5.3	23.0	19.5	10.0	0.25
#3 in EX1(c)	7.2	20.0	19.5	10.0	0.25

Table 2 Safety factors for the EX1(a) and EX(c) slope from different methods

No.	Method	FOS of EX1(a)	FOS of EX1(c)
1	Bishop	0.993	1.406
2	Janbu	0.978	1.325
3	Proposed method	0.988	1.283
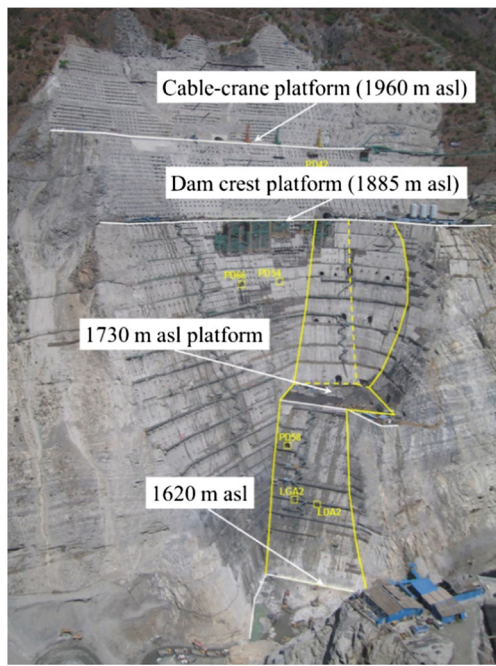
Fig. 3 Left bank slope of the Jinping first stage hydropower station excavated to 1620 m a.s.l.

is conservative relative to the LEMs, which is advantageous to estimate the stability of the steady slopes.

Left bank slope of the Jinping first stage hydropower station

The proposed method was applied to the stability analysis of the left bank slope of the Jinping first stage hydropower station. Due to the complexity of the slope, 3D FEM methods are difficult to address the mechanical relationship between the reinforcements and rock masses. Employing the SRM is time consuming because the elastoplastic state must be simulated for every strength reduction step during every excavation step. In contrast, the proposed method is convenient and efficient for obtaining the safety factor of the complex rock slope with reinforcements.

The Jinping first stage hydropower station is located in Sichuan Province, P. R. China. With an elevation of 305 m, this station is currently the highest double-curvature arch dam in the world. The total storage capacity of the reservoir is 7.76 billion m^3, the installed plant capacity is 3600 MW, and the annual power generation is 16.62 billion kW·h. The heights of the slopes on both sides of the dam site are both over 1000 m. The dip angles of the natural slopes below the dam crest elevation are greater than 60°. The excavation

Fig. 4 Geological profile of the left bank slope of the Jinping first stage hydropower station
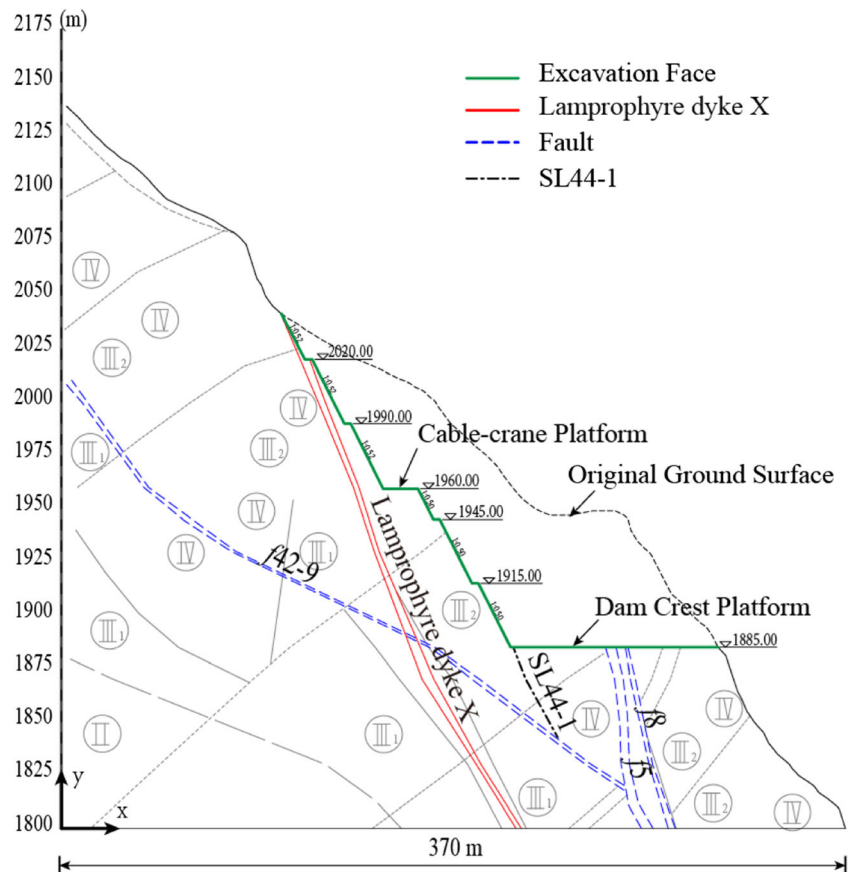
Table 3 Material parameters of the rock mass and key discontinuities

Items			ρ (kg/m^3)	c (MPa)	$\tan\varphi$	E (GPa)	ν
Rock quality grade		II	2800	2.00	1.35	26.0	0.25
		III$_1$	2800	1.50	1.07	11.5	0.25
		III$_2$	2800	0.90	1.02	6.5	0.30
		IV	2750	0.60	0.58	3.0	0.35
	f_5/f_8	Above 1680 m	2600	0.02	0.30	1.1	0.35
		Below 1680 m	2800	0.90	1.02	6.5	0.30
	Dyke X	Above 1680 m	2600	0.02	0.30	1.1	0.35
		Below 1680 m	2800	0.90	1.02	6.5	0.30
f_{42-9}			2750	0.02	0.30	0.4	0.35
Fissure SL_{44-1}			2750	0.40	0.40	0.4	0.35

height of the left bank slope is approximately 530 m, and the excavation volume is more than 5.5 million m^3. The construction of the left bank slope was one of the most challenging slope engineering projects in China. Figure 3 is a photo of the left bank slope excavated to 1620 m a.s.l.

Geologic setting

The left bank slope trends toward approximately N25°E and lies in the southeastern limb of the tight Santan syncline. The main strata are metamorphic rocks of the Zagunao Group of Middle to Upper Triassic age, whose main components are metasandstone and slate. In most areas of the slope, the bedrocks outcrop to the surface. Some local areas are covered by a layer of detritus soil. The weathering effect is very strong. Some dumping deformation in varying degrees exists among the superficial rock masses. The depths of strong and weak unloading zone range from 50 to 90 m and 100 to 160 m, respectively. The natural slope is stable. The geological conditions are very complex because of the existence of intersectional faults, dykes and fissures. The main discontinuities

controlling the stability of the left bank slope include the lamprophyre dyke X, the fissure SL44–1 and the faults f5, f8, and f42–9. A geological profile is shown in Fig. 4, in which the rock quality grades are classified according to the Standard for Engineering classification of rock masses of China (GB 50218–94).

The lamprophyre dyke X outcrops on both sides of the river valley. It extends more than 1000 m at a general attitude of 320~345°∠60~75°and a thickness of between 2 and 3 m. The posttectonic movement makes the interface between the dyke and surrounding rocks develop to be small faults.

Fault f5 enters the dam site from upstream and its exposed length reaches 1500 m. It is a strike-slip thrust fault with a displacement of 70–90 m that trends N40–50°E and dips SE70–80°. The properties of the shattered zone differ significantly as a function of the location and the lithology. The thickness ranges from 0.5 to 6 m. The main material compositions of crushed zones are fault breccia and rock debris.

Fault f8 is approximately 1.4 km long and 1–2 m thick. It meets fault f5 behind the excavation face. The attitude of the fault plane is 300~310°∠60~75°. The fault crushed zones consist of tectonic breccia, mylonite, and fault gouge.

Fig. 5 Potential sliding mass before (*left*) and after (*right*) excavation
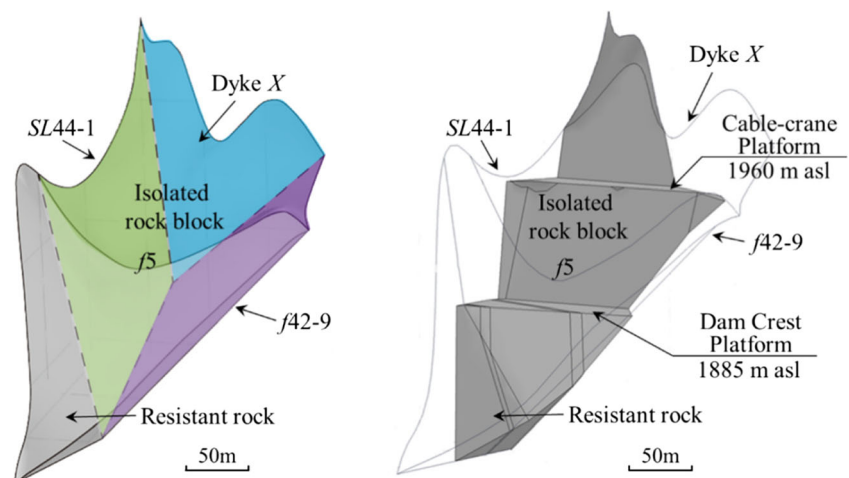
Table 4 Parameters of the prestressed anchor cables

Cable length (m)	Pullout load (kN)	Spacing (m)	Yield strength (MPa)	Number of strands	Anchored part length (m)
60	2000	5 × 5 m	1860	$12\phi15.24$ mm	12
80	3000	5 × 5 m	1860	$19\phi15.24$ mm	12

Fault $f42$–9 is the main discontinuity in the downstream slope, although its thickness is less than 1 m. Its extension to the valley is restricted by fault $f5$. In addition, the general attitude is 350~358°∠39~51°. The crushed zones mainly contain tectonic breccia, rock debris, and fault gouge.

SL44–1 is a tension fissure between fault $f5$ and dyke X and above fault $f42$–9, without any filler. Its general attitude is 80°∠52~65°, and its connectivity ratio is 50%.

The material parameters of the rock mass and key discontinuities are given in Table 3. The rock mass quality grades given in Table 3 correspond to those in Fig. 4.

Potential sliding mass

According to Zhou et al. (2006), the probability of failure of the left bank slope near the dam is the highest because the rock block is isolated by fault $f5$, fault $f42$–9, dyke X and fissure XL44–1, just behind the excavation face. The strength of fault $f42$–9 and dyke X is so low that the rock block tends to slide toward the valley along fault $f42$–9. Because fault $f42$–9 terminates at fault $f5$, the rock mass outside fault $f5$ prevents further movement of the block. However, when the slope is excavated to a level lower than the block, the resistance is significantly weakened. When the resistance of the rock is insufficient to support the block, it shears through the resisting

rock and slides out along fault $f42$–9. Figure 5 shows the two parts of the sliding mass, the isolated block and the resistant rock.

Reinforcement measures

Several slope stabilizing methods have been implemented to strengthen the left bank slope. These measures include a drainage system, anchor bolts, shotcreting, concrete lattices, anti-sliding piles, prestressed anchor cables and anti-shear cavities. Only the last two reinforcement measures relate to the potential sliding mass discussed previously. Therefore, only these will be taken into consideration in the following simulation.

Prestressed anchor cables were installed on the entire excavation face. Anti-corrosion steel strands with multiple anchor heads were employed. The pullout loads for the 6 and 80 m long prestressed anchor cables were 2000 and 3000 kN, respectively. The length of the anchored portion was 12 m, the inclination was 8°, and the spacing between the cables was 5 m in both the horizontal and vertical directions. The basic physical parameters for the prestressed anchor cables are listed in Table 4.

Anti-shear cavities were used to replace the material near the fault $f42$–9 with reinforced concrete. The size of their cross section is 9 m (width) × 10 m (height). Three anti-shear

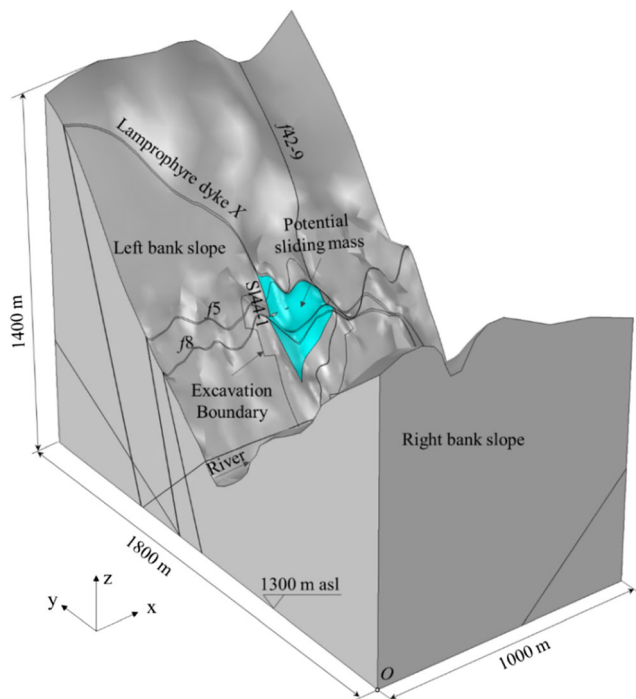**Fig. 6** The plan of the anti-shear cavity at 1834 m a.s.l.
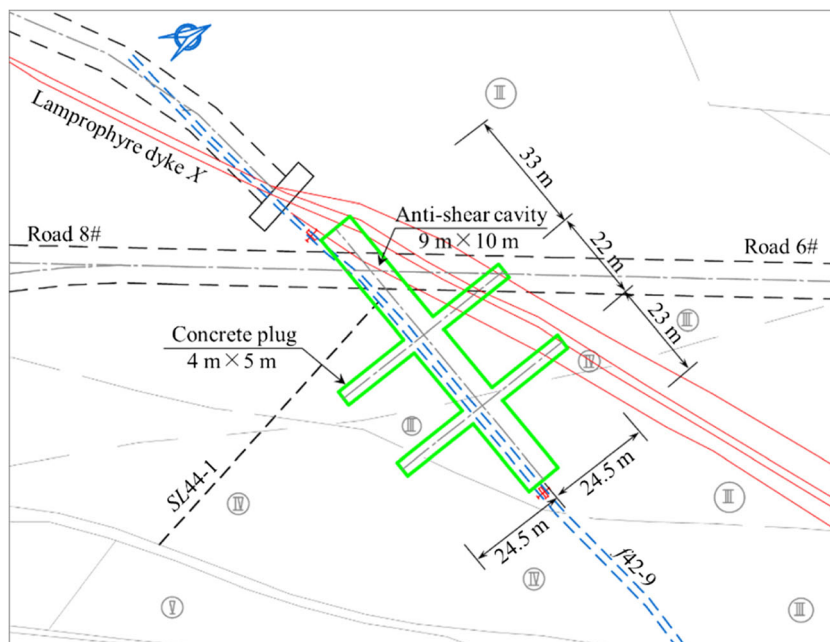
Table 5 Parameters of the concrete in the anti-shear cavities

Density (kg/m^3)	Young's modulus (GPa)	Poisson's ratio	Cohesion (MPa)	Internal friction angle (°)
2700	26	0.2	1	45

cavities were constructed at elevations of 1883, 1860, and 1834 m with lengths of 110, 90, and 78 m, respectively. Two 20-m-long concrete plugs were set up on each horizontal side of the lower two anti-shear cavities. A plan view of the anti-shear cavity at 1834 m a.s.l. is shown in Fig. 6. The basic physical and mechanical parameters of the reinforced concrete in the cavities are listed in Table 5.

Numerical simulation

The FEM software used to simulate the stresses of the left bank slope is Comsol Multiphysics V4.2. All the equations for calculating safety factors of each excavation steps are compiled in the software in advance. A dam-centered 3D model is constructed that includes both the left and right bank slopes, as shown in Fig. 7. The length in the x direction is 1000 m along the river, the width in y direction is 1800 m perpendicular to the valley, and the height is 1400 m, from 1300 to 2700 m a.s.l. A total of 618,533 elements are meshed for the model. To optimize the grids of the model, prism and tetrahedron elements are used for the structural planes and rock masses, respectively. The bottom boundary of the model is fixed and the normal displacements of all the lateral boundaries are constrained. The initial stress of the model is gravitational

stress. The prestressed anchor cables and anti-shear cavities are built in the model before calculating, and they will be enabled at the corresponding excavation steps. The structural elements are used to simulate the prestressed anchor cables. The strains between the prestressed anchor cables and the rock masses are coupled to make sure the deformation is compatible.

Duncan (1996) indicated that if the conditions were not close to failure, the differences between the factors of safety calculated using the elastoplastic and elastic stress–strain relationships would not be significant. Ge (2010) also came to a similar conclusion using the VSM. To save computational resources, the elastic theory is used here to calculate the stress tensor on the potential failure surface. Four conditions will be simulated: (1) excavation without any reinforcement, (2) excavation reinforced by prestressed anchor cables alone, (3) excavation reinforced by anti-shear cavities alone, and (4) excavation reinforced by a combination of both prestressed anchor cables and anti-shear cavities.

The whole excavation process from 2110 to 1580 m a.s.l. is divided into 11 steps. The height of the first step is 30 m, and that of all the others are 50 m. The cable-crane platform and the dam crest platform are also considered in the excavation sequence. The installation of prestressed anchor cables is synchronized with the excavation steps. In other words, when

Fig. 7 Geometry model for the simulation
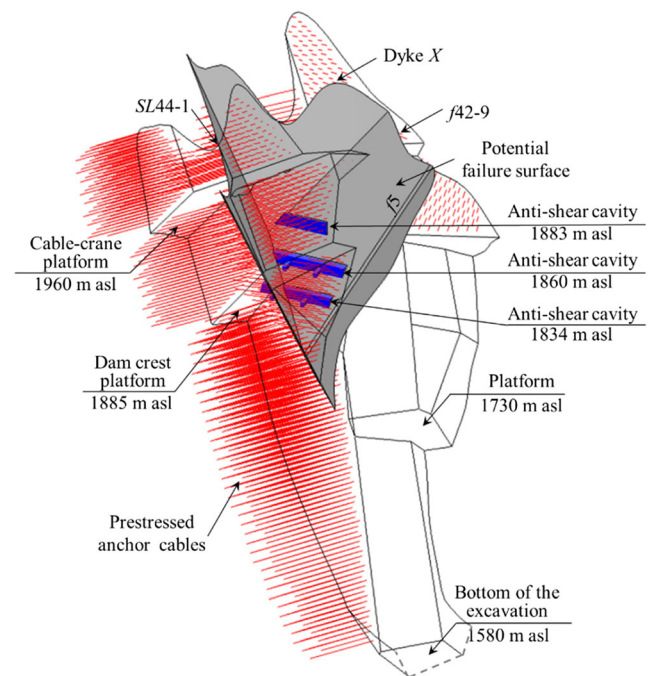
Fig. 8 Location of the anti-shear cavities, prestressed anchor cables, potential failure surface, and excavation faces

Fig. 9 Safety factors under different reinforcement conditions during excavation
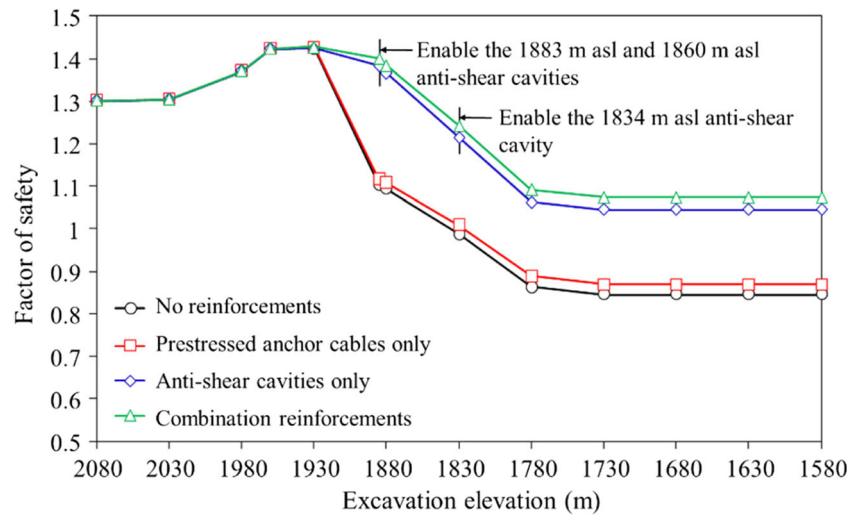
excavating for a certain step, the prestressed anchor cables above the excavation elevation in question are enabled. The construction of anti-shear cavities at the elevations of 1883 and 1860 m will be finished before excavating to dam crest platform. The 1834 m a.s.l. anti-shear cavity will be completed before excavation is begun at 1830 m a.s.l. The locations of the potential failure surface, the excavation face and the reinforcements are shown in Fig. 8.

Results

Stability under different reinforcement conditions

After obtaining the stress tensor on the potential failure surface, the factor of safety and the potential sliding direction can be calculated using Eqs. (16) and (11), respectively. However, some small treatments are to be applied for different reinforcement situations. When supported by anti-shear cavities, the potential failure surface is assumed to cut through the cavities along the original surface of fault $f42$–9. When taking into account the resistance of the anchor cables, Eq. (16), at this state, should be amended to be:

$$k = \frac{|\mathbf{F_r}| + \sum_i n_i \left(F_{mi} - F_{pi} \right)}{|\mathbf{F_s}|} \qquad (17)$$

where i is an index for the prestressed anchor cables ($i = s$ for the 60-m-long cables and l for the 80-m-long cables), n is the number of effective prestressed anchor cables intersecting with the potential failure surface, F_m is the yield force of a single cable and F_p is the pullout load. The changes of the safety factors with the excavation steps are shown in Fig. 9.

As shown in Fig. 9, the initial safety factor was 1.3 at the beginning of the excavation. There is no change in the safety factor before excavating the dam crest platform, regardless of

Fig. 10 Average normal stress of the potential failure surface under different reinforcements during excavation
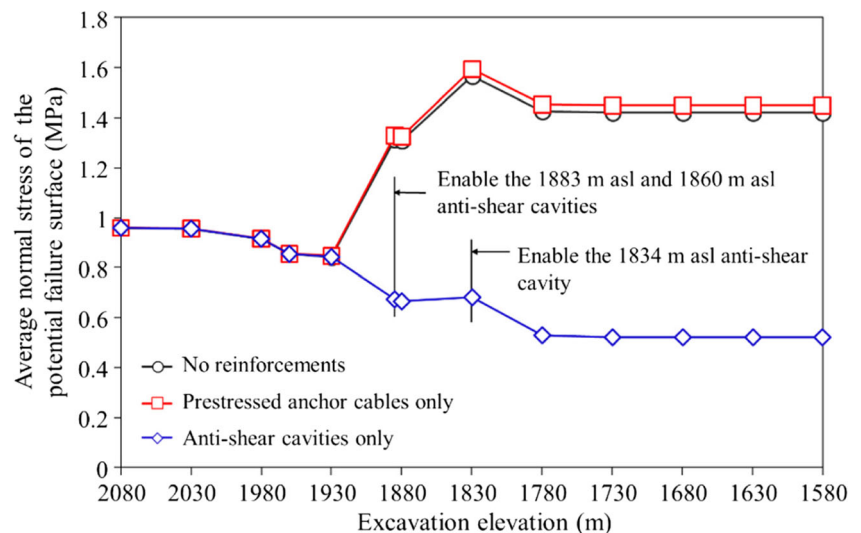
Fig. 11 Average shear stress of
the potential failure surface under
different reinforcements during
excavation
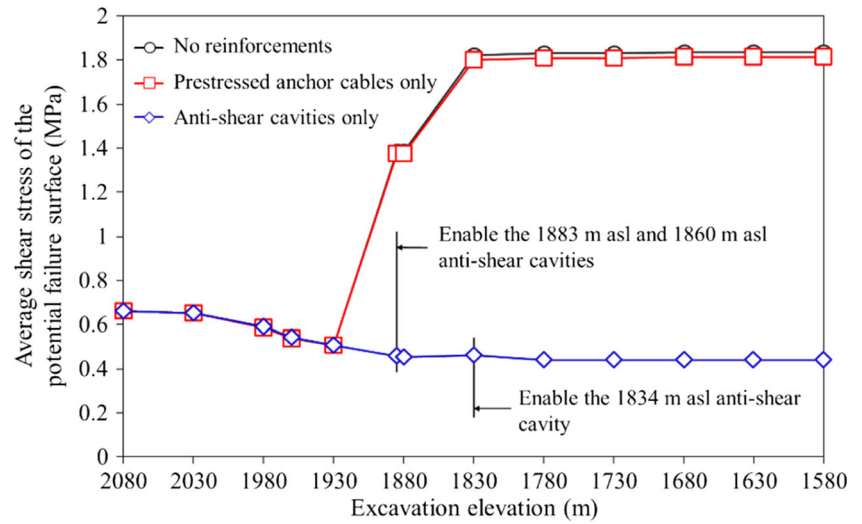
the reinforcement conditions. The safety factor increased with
the first few excavation steps because the removal of the rock
mass was equivalent to an unloading process.

Without reinforcement, the safety factor decreased sharply
when excavating from 1930 m a.s.l. to the dam crest platform
(1885 m a.s.l.). This is due to the reduction in the resistance of
the rock outside fault *f*5. When the excavation elevation was
1830 m a.s.l., the safety factor reached a value lower than 1,
which implies that the excavation was at an unstable state. As

the excavation continued to lower heights, to 1730 m a.s.l. and
below, it was found that the safety factor was no longer de-
pendent on the excavation process at all.

The reinforcing ability of prestressed anchor cables on the
discussed failure mode was quite limited. They only improved
the safety factor by 2.5%. The anti-shear cavities, on the other
hand, played a prominent role in improving the stability of the
slope. The addition of anti-shear cavities at 1883 and 1960 m
a.s.l. effectively maintained the safety factor at a level higher

Fig. 12 Angles between the
potential sliding direction and the
axes
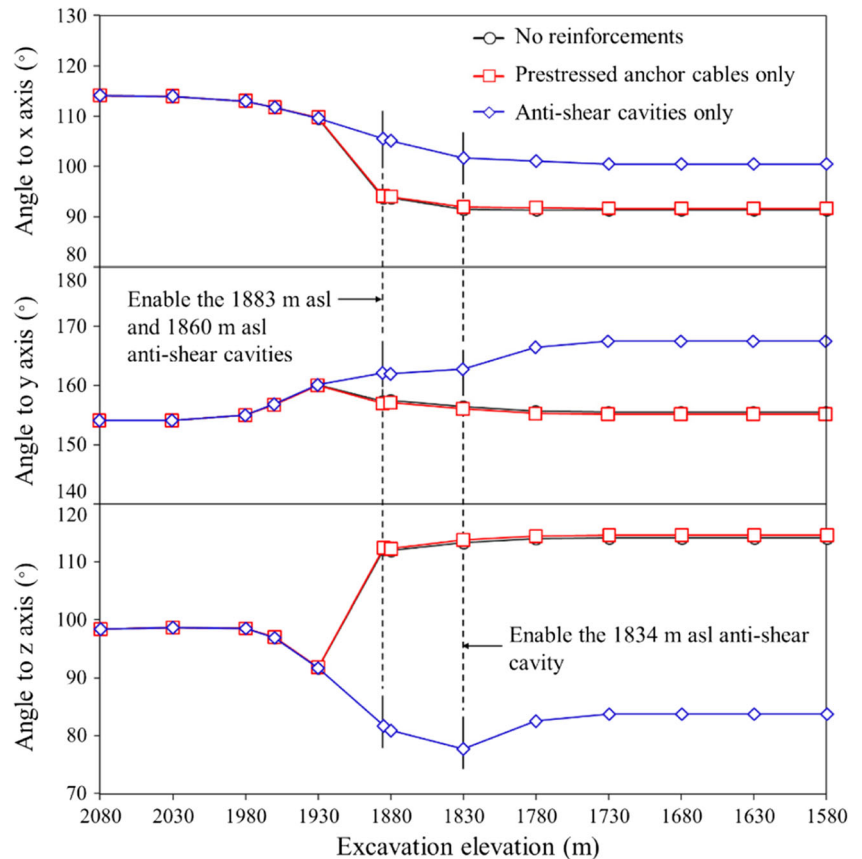
Fig. 13 Angles between the potential sliding direction and the normal vector of fault f42–9
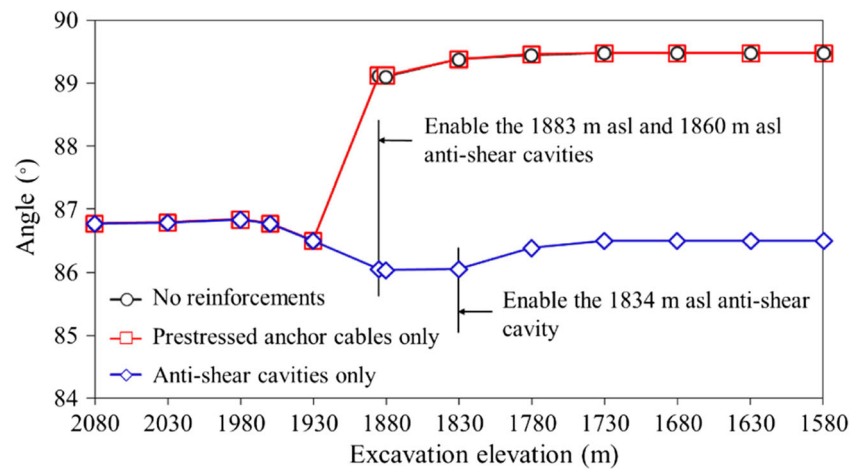
than 1. The results from a combination of the prestressed anchor cables and the anti-shear cavities were found to be slightly better than the superposition of their respective results.

Influence of different reinforcement measures on the slope stability

The influence of different reinforcement measures on the average normal stress and average shear stress of the potential failure surface are depicted in Figs. 10 and 11, respectively.

When prestressed anchor cables were used, the average normal stress became bigger, and the average shear stress became smaller than that of conditions without any reinforcement at every excavation step below 1930 m a.s.l. However, their amplitudes were so small that the impact on the safety factor was slight.

When anti-shear cavities were enabled, both the average normal stress and shear stress on the potential failure surface continued to decline because the anti-shear cavities restricted the movement of the unstable rock blocks isolated by the discontinuities. Although the resistant rocks outside fault f5 were excavated, the unstable rock blocks did not require the resistant rocks to provide resistance any longer.

Using the potential sliding direction obtained from Eq. (11), the angles between the potential sliding direction and the axes were computed and are shown in Fig. 12. The most likely sliding direction was predicted to occur along fault f42–9. The angles between the normal vector of fault f42–9 and the x, y, and z coordinates were 94.3, 92.3, and 85.9°, respectively. The angles between the potential sliding direction and the normal vector of fault f42–9 are plotted in Fig. 13. From these two figures, it can be observed that the influence of the prestressed anchor cables on the potential sliding direction was very inconspicuous, which was expected.

In Fig. 13, if the angle was close to 90°, the potential sliding direction approached perpendicular to the normal vector of

fault f42–9 and thereby was parallel to the tangential direction of fault f42–9. When excavating from 1930 m a.s.l. to the dam crest platform (1885 m a.s.l.), the potential sliding direction dramatically shifted to the tangential direction of fault f42–9. The prestressed anchor cables could not reverse this situation. However, the effect of the anti-shear cavities was significant because they prevented the potential sliding direction from escalating to a worse condition.

Overall, the combined reinforcements of the prestressed anchor cables and the anti-shear cavities efficiently restricted the deformation and ensured the stability of the left bank slope of the Jinping first stage hydropower station during the excavation process. The contribution of the anti-shear cavities was found to be much greater than that of the prestressed anchor cables. The same qualitative assessment was drawn by Li et al. (2015a) through the reliability analysis of the same failure mode with these two reinforcement measures. In their study, the average safety factors of the same failure mode are 1.346 and 1.172 when excavated to 1780 m with reinforcement or not. However, evaluated by the proposed method, the nature slope without any reinforcement has failed when excavated to 1830 m. Therefore, the evaluation of the proposed method is conservative compared with the results obtained by Li et al. (2015a), which is more advantageous to ensure the safety during engineering construction.

Discussion

For LEMs and SRMs, the potential sliding direction is not a necessary part for the calculation of the factor of safety. However, as to the proposed method in this paper, the potential sliding direction concerns the projection results of the resistance force and the sliding force. The potential sliding direction calculated is assumed to be the reverse direction of the resultant force of the shear stress acting on the potential failure surface. A more reasonable definition of the potential

sliding direction with clear mechanical meanings should be studied in the future.

In the case study, the elastic theory is utilized to obtain the stress on the potential failure surface. If using elastoplastic theory, the results will be more accurate. Even though the pre-stressed anchor cables make little difference on the stability of the potential failure mode chosen in this paper, they are an essential part for the whole stability of the left bank slope of Jinping first stage hydropower station. The effect of the pre-stressed anchor cables cannot be underestimated according to the results in this paper.

Conclusions

In order to analyze the stability of complex rock slopes with multiple discontinuities and reinforcements, an evaluation method of slope stability is proposed in this paper, and it was applied to the stability analysis of the left bank slope of the Jinping first stage hydropower station. The stress on potential sliding surface was calculated by FEM method. The excavation process before and after reinforcing was simulated. The following conclusions can be drawn:

(1). The proposed method is established based on the actual stress state of the potential failure surface. All the equations calculating the safety factor can be applied in both 2D and 3D situations. The influence of the potential sliding direction on slope stability is considered, which is meaningful to guide the adoption of reinforcement scheme.

(2). EX1(a) and EX1(c) released by ACAD are used to examine the proposed method. The results show that the proposed method can correctly evaluate the critical state of a slope, and for safe slopes, the proposed method is conservative compared with LEMs.

(3). The reinforcement effects of pre-stress anchor cables and anti-shear cavities of the left bank slope of Jinping first stage hydropower station are evaluated by the proposed method. The results indicate that the natural slope will be instable when excavated to 1830 m without any reinforcement. The combination of these two reinforcements can ensure the stability of the selected failure mode during the whole excavation process, and the anti-shear cavities are more effective than the pre-stressed anchor cables for the stability. The proposed method is feasible for evaluating the stability of complex 3D rock slopes with reinforcements.

References

Ausilio E, Conte E, Dente G (2001) Stability analysis of slopes reinforced with piles. Comput Geotech 28:591–611

Bishop AW (1955) The use of the slip circle in stability analysis of slope. Géotechnique 5:7–17

Chen J, Liu J, Xue J-F, Shi Z (2014) Stability analyses of a reinforced soil wall on soft soils using strength reduction method. Eng Geol 177: 83–92

Dawson EM, Roth WH, Drescher A (2000) Slope stability analysis by strength reduction. Geotechnique 49:835–840

Donald IB, Giam P (1992) The ACADS Slope Stability Programs Review. 6th International Symposium on Landslides, Vol. 3, 1665–1670

Duncan M (1996) State of the art: limit equilibrium and finite-element analysis of slopes. J Geotech Eng 122:577–596

Ge X-R (2010) The vector sum method: a new approach to calculating the safety factor of stability against sliding for slope engineering and dam foundation problems. In: Chen Y, Zhan L, Tang X (Eds) Advances in Environmental Geotechnics: Proceedings of the International Symposium on Geoenvironmental Engineering in Hangzhou, China, September 8–10, 2009. Springer Berlin Heidelberg, Berlin, Heidelberg, pp 99–110

Gupta V, Bhasin RK, Kaynia AM et al (2015) Finite element analysis of failed slope by shear strength reduction technique: a case study for Surabhi resort landslide, Mussoorie Township, Garhwal Himalaya. Geomat Nat Hazards Risk 5705:1–14

Hammah RE, Yacoub TE, Corkum B, Wibowo F, Curran JH (2007) Analysis of blocky rock slopes with finite element shear strength reduction analysis. In: Eberhardt E, Stead D, Morrison T (Eds) Proceedings of the 1st Canada-US Rock Mechanics Symposium in Vancouver, Canada, 27–31 May 2007. CRC Press, London, pp 329–334

Huang R, Lin F, Yan M (2010) Deformation mechanism and stability evaluation for the left abutment slope of Jinping I hydropower station. Bull Eng Geol Environ 69:365–372

Janbu N (1975) Slope stability computations. Int J Rock Mech Min Sci Geomech Abstr 12:67

Kalatehjari R, Ali N (2013) A review of three-dimensional slope stability analyses based on limit equilibrium method. Electron J Geotech Eng 18 A:119–134

Kelesoglu MK (2016) The evaluation of three-dimensional effects on slope stability by the strength reduction method. KSCE J Civ Eng 20:229–242

Li D, Jiang S, Cao Z et al (2015a) Efficient 3-D reliability analysis of the 530m high abutment slope at Jinping I Hydropower Station during construction. Eng Geol 195:269–281

Li T, He J, Zhao L et al (2015b) Strength reduction method for stability analysis of local discontinuous rock mass with iterative method of partitioned finite element and interface boundary element. Math Probl Eng 2015:11

Lu L, Wang Z, Song M, Arai K (2015) Stability analysis of slopes with ground water during earthquakes. Eng Geol 193:288–296

Nian TK, Huang RQ, Wan SS, Chen GQ (2012) Three-dimensional strength-reduction finite element analysis of slopes: geometric effects. Can Geotech J 49:574–588

Piteau D (1972) Engineering geology considerations and approach in assessing the stability of rock slopes. Bull Assoc Eng Geol IX 301–320

Price V, Morgenstern N (1968) The analysis of the stability of general slip surfaces. Géotechnique 18:393–394

Qi S, Wu F, Yan F, Lan H (2004) Mechanism of deep cracks in the left bank slope of Jinping first stage hydropower station. Eng Geol 73: 129–144

Qi S, Wu F, Zhou Y et al (2010) Influence of deep seated discontinuities on the left slope of Jinping I Hydropower Station and its stability analysis. Bull Eng Geol Environ 69:333–342

Roosta RM, Sadaghiani MH, Pak A (2005) Strength reduction technique in stability analysis of jointed rock slopes. Int J Civ Eng 3:152–165

Sarma SK (1979) Stability analysis of embankments and slopes. J Geotech Eng Div GT12:1511–1524

Spencer E (1976) A method of analysis of the stability of embankments assuming parallel inter-slice forces. Géotechnique 17:11–26

Su H, Hu J, Yang M (2014) Evaluation method for slope stability under multianchor support. Nat Hazards Rev 16:4014034

Sun G, Zheng H, Huang Y (2015) Stability analysis of statically indeterminate blocks in key block theory and application to rock slope in Jinping-I Hydropower Station. Eng Geol 186:57–67

Sun G, Cheng S, Jiang W, Zheng H (2016) A global procedure for stability analysis of slopes based on the Morgenstern-price assumption and its applications. Comput Geotech 80:97–106

Sun G, Yang Y, Cheng S, Zheng H (2017) Phreatic line calculation and stability analysis of slopes under the combined effect of reservoir water level fluctuations and rainfall. Can Geotech J 54(5):631–645

Wei WB, Cheng YM (2009) Strength reduction analysis for slope reinforced with one row of piles. Comput Geotech 36:1176–1185

Won J, You K, Jeong S, Kim S (2005) Coupled effects in stability analysis of pile-slope systems. Comput Geotech 32:304–315

Xia M, Ren G, Zhu S, Ma X (2015) Relationship between landslide stability and reservoir water level variation. Bull Eng Geol Environ 74(3):909–917

Zhou Z, Gong M, Lei C (2006) Research on stability of slope at left abutment of Jinping first stage hydropower station. Chin J Rock Mech Eng 25:2298–2304 **(in Chinese)**

Zhu DY, Lee CF, Chan DH, Jiang HD (2005) Evaluation of the stability of anchor-reinforced slopes. Can Geotech J 42:1342–1349

Zienkiewicz OC, Humpheson C, Lewis RW (1975) Associated and non-associated visco-plasticity and plasticity in soil mechanics. Géotechnique 25:671–689